

A Multiscale Dynamo Model Driven by Quasi-geostrophic Convection

By Michael A. Calkins¹ *, Keith Julien¹, Steven M. Tobias², and Jonathan M. Aurnou³

¹Department of Applied Mathematics, University of Colorado, Boulder, CO 80309, USA

²Department of Applied Mathematics, University of Leeds, Leeds, UK LS2 9JT

³Department of Earth, Planetary and Space Sciences, University of California, Los Angeles, CA 90095, USA

(Received ?; revised ?; accepted ?. - To be entered by editorial office)

A convection-driven multiscale dynamo model is developed for the plane layer geometry in the limit of low Rossby number. The small-scale fluctuating dynamics are described by a magnetically-modified quasi-geostrophic equation set, and the large-scale mean dynamics are governed by a diagnostic thermal wind balance. The model utilizes three timescales that respectively characterize the convective timescale, the large-scale magnetic diffusion timescale, and the large-scale thermal diffusion timescale. Distinct equations are derived for the cases of order one and low magnetic Prandtl number. It is shown that the low magnetic Prandtl number model is characterized by a magnetic to kinetic energy ratio that is asymptotically large, with ohmic dissipation dominating viscous dissipation on the large-scales. For the order one magnetic Prandtl number model the magnetic and kinetic energies are equipartitioned and both ohmic and viscous dissipation are weak on the large-scales; large-scale ohmic dissipation occurs in thin magnetic boundary layers adjacent to the solid boundaries. For both magnetic Prandtl number cases the Elsasser number is small. The new models can be considered fully nonlinear, generalized versions of the dynamo model originally developed by Childress and Soward [Phys. Rev. Lett., **29**, p.837, 1972]. These models may be useful for understanding the dynamics of convection-driven dynamos in regimes that are only just becoming accessible to simulations of the full set of governing equations.

1. Introduction

It is now generally accepted that many of the observed planetary and stellar magnetic fields are the result of convectively driven dynamos (Miesch 2005; Stanley & Glatzmaier 2010). Direct numerical simulations (DNS) of the complete set of governing equations are now routine practice, but remain limited to parameter values that are quite distant from natural systems owing to the massive requirements for numerically resolving disparate spatiotemporal scales (e.g. Jones 2011). The stiff character of the governing equations, while an impediment to DNS, provides a possible path forward for simplifying, or reducing, the governing equations with the use of multiscale asymptotics (e.g. Julien & Knobloch 2007; Klein 2010). Balanced flows, in which two or more forces in the momentum equations are in balance, are particularly suitable for asymptotic analysis given the subdominance of inertial accelerations. Indeed, reduced models based on the geostrophic balance, in which the Coriolis and pressure gradient forces balance, have

* Email address for correspondence: michael.calkins@colorado.edu

formed the backbone for theoretical and numerical investigations on the dynamics of the Earth’s atmosphere and oceans for over 60 years (Charney 1948; Pedlosky 1987).

It is an unfortunate fact, however, that direct measurements of the forces present within the electrically conducting regions of natural systems are not possible. That most large-scale planetary and stellar magnetic fields are aligned with their respective rotation axes (e.g. Schubert & Soderlund 2011) suggests that the Coriolis force plays a key role in the magnetic field generation process, at least with respect to the large-scale dynamics. For the case of the Earth’s liquid outer core, viscous stresses are likely to be small for large-scale motions there (Pozzo *et al.* 2013), and observations tracking the movement of the geomagnetic field show that typical convective timescales are significantly longer than the rotation period (Finlay & Amit 2011). These studies suggest that large-scale dynamics within the core may be geostrophically balanced (Jault *et al.* 1988; Jackson *et al.* 1993; Nataf & Schaeffer 2015). Alternatively, if the magnetic field is sufficiently strong within the core, it is possible that the Lorentz force can balance with the Coriolis and pressure gradient forces to yield magnetostrophically balanced motions at certain length-scales (Roberts 1988; Moffatt 2008; King & Aurnou 2015). It can be argued that only geostrophically balanced dynamos have been observed with DNS (Soderlund *et al.* 2012; King & Buffett 2013).

In a seminal investigation, Childress & Soward (1972) (denoted CS72 hereafter) demonstrated that laminar convection in a rotating plane layer geometry is capable of supporting dynamo action. CS72 outlined three unique distinguished limits, or balances, in the governing equations that can occur based on the relative strength of the magnetic field, which they referred to as the weak field, intermediate field, and strong field limits. Soward (1974) (denoted S74 hereafter) investigated the so-called weak field limit in detail by assuming the flow was weakly nonlinear. Fautrelle & Childress (1982) later showed that weak field states may be unstable. We refer to the weak-field model studied by S74 as the Childress-Soward dynamo model, denoted by CSDM. The basis for the CSDM is that the Ekman number $E_H = \nu/\Omega H^2$ is taken as a small parameter, where ν is the kinematic viscosity, Ω is the rotation rate and H is the depth of the fluid layer. In this case convection is spatially anisotropic with large aspect ratio $H/\ell \gg 1$, where ℓ characterizes the small horizontal length scale of the convection (Chandrasekhar 1961). By expanding the flow variables in powers of $E^{1/6}$, a dynamical equation for the large-scale horizontal magnetic field is derived that is driven by the electromotive force (emf) generated by the small-scale fluctuating velocity and magnetic fields. Because the CSDM utilizes a single time scale, it applies to order one thermal and magnetic Prandtl numbers, $Pr = \nu/\kappa$ and $Pm = \nu/\eta$, respectively, where κ is the thermal diffusivity and η is the magnetic diffusivity of the fluid.

The CSDM continues to provide an invaluable tool for understanding the differences between large-scale and small-scale dynamo action, as well as aiding the interpretation of results obtained from DNS studies. S74 showed that a dynamo driven by small-scale rapidly rotating convection is necessarily large-scale. Many of the key features predicted by S74, such as the vertical structure and temporal evolution of the large-scale magnetic field, have been confirmed with low Ekman number DNS (e.g. Stellmach & Hansen 2004). Recent work has employed the CSDM for investigating kinematic dynamo action driven by rotating convection (Favier & Proctor 2013). Mizerski & Tobias (2013) have extended the CSDM to include the effects of fluid compressibility via the anelastic approximation, showing that density stratification tends to delay the onset of dynamo action and reduces the strength of the resulting magnetic field.

In the present work we develop a new multiscale dynamo model that possesses many similarities with the CSDM, but also significant differences. We refer to the new model as

the quasi-geostrophic dynamo model, or QGDM. Like the weak field CSDM, the small-scale, convective dynamics are geostrophically balanced to leading order, but remain time-dependent and fully nonlinear in the QGDM; our small-scale dynamical equations are a magnetically modified version of the quasi-geostrophic convection equations developed by Julien *et al.* (1998) (see also Julien *et al.* (2006) for a generalized development). In addition to the small horizontal convective lengthscale ℓ , the QGDM includes large-scale horizontal modulations L_X that allow for a diagnostic thermal wind balance in the large-scale momentum equations. Coupled with the large-scale heat equation, the large-scale model (in the absence of a magnetic field) is the equivalent of the planetary geostrophic equations commonly employed in oceanography (Robinson & Stommel 1959; Welander 1959) and atmospheric science (Phillips 1963; Dolaptchiev & Klein 2009). (The so-called β -effect has been neglected in the present work though it can easily be incorporated into the current model, e.g. see Grooms *et al.* (2011)). Because of the additional scale L_X , the QGDM also possesses a non-zero large-scale vertical magnetic field that is not present in the CSDM. Moreover, the new model utilizes three disparate timescales characterizing the small-scale convective dynamics, the large-scale magnetic diffusion timescale, and the large-scale thermal diffusion timescale. Both low and order one magnetic Prandtl number cases are considered. The QGDM can be simulated numerically to gain insight on large-scale magnetic field generation in planets and stars, where we can utilize the success of previous non-magnetic work (e.g. Sprague *et al.* 2006; Julien *et al.* 2012*a,b*; Rubio *et al.* 2014; Stellmach *et al.* 2014), and the increases in computational power that have occurred since the work of CS72.

In section 2 we present the asymptotic development of the model, in section 3 we discuss some of the important features of the QGDM and its relationship with the CSDM, and concluding remarks are given in section 4.

2. Model Development

2.1. Governing Equations

We consider a rotating plane layer geometry with rotation vector $\mathbf{\Omega} = \Omega \hat{\mathbf{z}}$ and constant gravity vector $\mathbf{g} = -g\hat{\mathbf{z}}$. The horizontal boundaries are located a vertical distance H apart with the layer heated from the bottom boundary and cooled at the top boundary. For simplicity, the fluid is assumed to be Newtonian and Boussinesq with density ρ and thermal expansion coefficient α . The governing equations are then non-dimensionalized utilizing the generic scales \mathcal{U} , ℓ , ℓ/\mathcal{U} , ΔT , \mathcal{P} and \mathcal{B} for the velocity, length, time, temperature, pressure, and magnetic field, respectively. In the rotating reference frame with coordinates (x, y, z) the dimensionless governing equations are then

$$\partial_t \mathbf{u} + \mathbf{u} \cdot \nabla \mathbf{u} + \frac{1}{Ro} \hat{\mathbf{z}} \times \mathbf{u} = -Eu \nabla p + M \mathbf{B} \cdot \nabla \mathbf{B} + \Gamma \theta \hat{\mathbf{z}} + \frac{1}{Re} \nabla^2 \mathbf{u}, \quad (2.1)$$

$$\partial_t \theta + \nabla \cdot (\mathbf{u} \theta) = \frac{1}{Pe} \nabla^2 \theta, \quad (2.2)$$

$$\partial_t \mathbf{B} = \nabla \times (\mathbf{u} \times \mathbf{B}) + \frac{1}{Rm} \nabla^2 \mathbf{B}, \quad (2.3)$$

$$\nabla \cdot \mathbf{u} = 0, \quad \nabla \cdot \mathbf{B} = 0, \quad (2.4)$$

where the velocity, pressure, temperature, and magnetic field are denoted by $\mathbf{u} = (u, v, w)$, p , θ , and $\mathbf{B} = (B, C, D)$, respectively. Both the hydrostatic centrifugal force and magnetic pressure have been absorbed in the pressure gradient term ∇p . The dimensionless

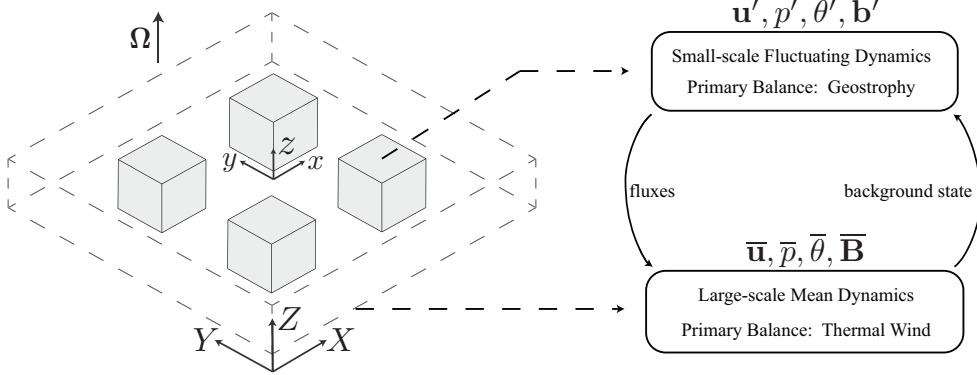


Figure 1: Schematic summarizing the general features of the multiscale dynamo model. The large-scale coordinate system is $\mathbf{X} = (X, Y, Z)$ and the small-scale coordinate system is $\mathbf{x} = (x, y, z)$; the shaded boxes depict small-scale subdomains embedded within the single large-scale domain. Large-scale mean dependent variables are given by $(\bar{\mathbf{u}}, \bar{p}, \bar{\theta}, \bar{\mathbf{B}})$ and the small-scale fluctuating dependent variables are $(\mathbf{u}', p', \theta', \mathbf{b}')$. Distinct equation sets are developed for the large-scale and small-scale domains, with the mean dynamics controlling the background state for the fluctuating dynamics and the fluctuating dynamics feeding back onto the mean state via small-scale fluxes.

parameters are defined by

$$Ro = \frac{\mathcal{U}}{2\Omega\ell}, \quad \Gamma = \frac{g\alpha\Delta T\ell}{\mathcal{U}^2}, \quad Re = \frac{\mathcal{U}\ell}{\nu}, \quad Pe = \frac{\mathcal{U}\ell}{\kappa}, \quad Eu = \frac{\mathcal{P}}{\rho\mathcal{U}^2}, \quad (2.5)$$

$$M = \frac{\mathcal{B}^2}{\rho\mu\mathcal{U}^2}, \quad Rm = \frac{\mathcal{U}\ell}{\eta}. \quad (2.6)$$

Here, Ro is the Rossby number, Γ is the buoyancy number, Re is the Reynolds number, Pe is the Péclet number, Eu is the Euler number, M represents the magnetic field strength, and Rm is the magnetic Reynolds number. The permeability of free space is denoted by μ . We recall that the thermal and magnetic Prandtl numbers characterizing the fluid properties are related to the above parameters via the relationships $Pe = RePr$ and $Rm = RePm$. Importantly, in the present work we denote dimensionless parameters that are based on the large-scale depth of the fluid layer with a subscript H , whereas parameters without this distinction refer to small-scale quantities.

In what follows we assume that the horizontal bounding surfaces are impenetrable, stress-free and perfect thermal and electrical conductors such that

$$\partial_z u = \partial_z v = w = \partial_z B = \partial_z C = D = 0, \quad \text{at } z = 0, H/\ell, \quad (2.7)$$

$$\theta = 1 \quad \text{at } z = 0, \quad \text{and} \quad \theta = 0 \quad \text{at } z = H/\ell. \quad (2.8)$$

The development given here parallels that of Julien & Knobloch (2007) and Grooms *et al.* (2011) for other multiscale models. We find that three disparate timescales are necessary to completely describe the temporal evolution of the dynamo; these are (1) the timescale of the small-scale convective fluctuations (denoted by t), (2) the large-scale magnetic diffusion timescale (τ), and (3) the large-scale thermal diffusion timescale (T). The small-scale, rapidly varying spatial and temporal coordinates are denoted as (\mathbf{x}, t) , and the slowly varying large-scale coordinates are given by (\mathbf{X}, τ, T) . The fields are de-

composed into mean and fluctuating components according to

$$\mathbf{u}(\mathbf{x}, \mathbf{X}, t, \tau, T) = \bar{\mathbf{u}}(\mathbf{X}, \tau, T) + \mathbf{u}'(\mathbf{x}, \mathbf{X}, t, \tau, T), \quad (2.9)$$

$$p(\mathbf{x}, \mathbf{X}, t, \tau, T) = \bar{p}(\mathbf{X}, \tau, T) + p'(\mathbf{x}, \mathbf{X}, t, \tau, T), \quad (2.10)$$

$$\theta(\mathbf{x}, \mathbf{X}, t, \tau, T) = \bar{\theta}(\mathbf{X}, \tau, T) + \theta'(\mathbf{x}, \mathbf{X}, t, \tau, T), \quad (2.11)$$

$$\mathbf{B}(\mathbf{x}, \mathbf{X}, t, \tau, T) = \bar{\mathbf{B}}(\mathbf{X}, \tau, T) + \mathbf{b}'(\mathbf{x}, \mathbf{X}, t, \tau, T), \quad (2.12)$$

and the fluctuating magnetic field vector is $\mathbf{b}' = (b', c', d')$. In Figure 1 a schematic illustrating the general features of the model is shown. The mean quantities are defined as averages taken over the fast scales according to

$$\bar{f}(\mathbf{X}, \tau, T) = \lim_{t', \mathcal{V} \rightarrow \infty} \frac{1}{t' \mathcal{V}} \int_{t', \mathcal{V}} f(\mathbf{x}, \mathbf{X}, t, \tau, T) d\mathbf{x} dt, \quad \bar{f}' \equiv 0, \quad (2.13)$$

with the small-scale fluid volume denoted by \mathcal{V} . With multiple scales the differentials become

$$\partial_t \rightarrow \partial_t + \frac{1}{A_\tau} \partial_\tau + \frac{1}{A_T} \partial_T, \quad (2.14)$$

$$\nabla \rightarrow \nabla + \bar{\nabla}, \quad (2.15)$$

where now ∇ only acts on the small-scale coordinates \mathbf{x} and the large-scale, mean gradient operator is defined by

$$\bar{\nabla} = \left(\frac{1}{A_X} \partial_X, \frac{1}{A_Y} \partial_Y, \frac{1}{A_Z} \partial_Z \right). \quad (2.16)$$

The various aspect ratios are defined according to

$$A_X = A_Y = \frac{L_X}{\ell}, \quad A_Z = \frac{H}{\ell}, \quad A_\tau = \frac{t}{\tau}, \quad A_T = \frac{t}{T}. \quad (2.17)$$

For simplicity we assume isotropic horizontal large-scale modulations (i.e. $A_X = A_Y$) in the present work, though the approach remains completely general.

The governing equations become

$$\begin{aligned} & \left(\partial_t + \frac{1}{A_\tau} \partial_\tau + \frac{1}{A_T} \partial_T \right) \mathbf{u} + \nabla \cdot (\mathbf{u} \mathbf{u}^{tr}) + \bar{\nabla} \cdot (\mathbf{u} \mathbf{u}^{tr}) + \frac{1}{Ro} \hat{\mathbf{z}} \times \mathbf{u} = \\ & -Eu (\nabla + \bar{\nabla}) p + M (\mathbf{B} \cdot \nabla + \mathbf{B} \cdot \bar{\nabla}) \mathbf{B} + \Gamma \theta \hat{\mathbf{z}} + \frac{1}{Re} (\nabla^2 + \bar{\nabla}^2) \mathbf{u}, \end{aligned} \quad (2.18)$$

$$\left(\partial_t + \frac{1}{A_\tau} \partial_\tau + \frac{1}{A_T} \partial_T \right) \theta + \nabla \cdot (\theta \mathbf{u}) + \bar{\nabla} \cdot (\theta \mathbf{u}) = \frac{1}{Pe} (\nabla^2 + \bar{\nabla}^2) \theta, \quad (2.19)$$

$$\left(\partial_t + \frac{1}{A_\tau} \partial_\tau + \frac{1}{A_T} \partial_T \right) \mathbf{B} = \nabla \times (\mathbf{u} \times \mathbf{B}) + \bar{\nabla} \times (\mathbf{u} \times \mathbf{B}) + \frac{1}{Rm} (\nabla^2 + \bar{\nabla}^2) \mathbf{B}, \quad (2.20)$$

$$(\nabla + \bar{\nabla}) \cdot \mathbf{u} = 0, \quad (\nabla + \bar{\nabla}) \cdot \mathbf{B} = 0. \quad (2.21)$$

The superscript “ tr ” appearing on some of the velocity vectors denotes a transpose.

Averaging the equations over fast temporal and spatial scales (\mathbf{x}, t) results in the mean equations

$$\begin{aligned} & \left(\frac{1}{A_\tau} \partial_\tau + \frac{1}{A_T} \partial_T \right) \bar{\mathbf{u}} + \bar{\nabla} \cdot (\bar{\mathbf{u}} \bar{\mathbf{u}}^{tr}) + \bar{\nabla} \cdot (\overline{\mathbf{u}' (\mathbf{u}')^{tr}}) + \frac{1}{Ro} \hat{\mathbf{z}} \times \bar{\mathbf{u}} = \\ & -Eu \bar{\nabla} \bar{p} + M \bar{\mathbf{F}}_L + \Gamma \bar{\theta} \hat{\mathbf{z}} + \frac{1}{Re} \bar{\nabla}^2 \bar{\mathbf{u}}, \end{aligned} \quad (2.22)$$

$$\left(\frac{1}{A_\tau}\partial_\tau + \frac{1}{A_T}\partial_T\right)\bar{\theta} + \bar{\nabla} \cdot (\bar{\theta}\bar{\mathbf{u}}) + \bar{\nabla} \cdot (\overline{\theta'\mathbf{u}'}) = \frac{1}{Pe}\bar{\nabla}^2\bar{\theta}, \quad (2.23)$$

$$\left(\frac{1}{A_\tau}\partial_\tau + \frac{1}{A_T}\partial_T\right)\bar{\mathbf{B}} = \bar{\nabla} \times (\bar{\mathbf{u}} \times \bar{\mathbf{B}}) + \bar{\nabla} \times (\overline{\mathbf{u}' \times \mathbf{b}'}) + \frac{1}{Rm}\bar{\nabla}^2\bar{\mathbf{B}}, \quad (2.24)$$

$$\bar{\nabla} \cdot \bar{\mathbf{u}} = 0, \quad \bar{\nabla} \cdot \bar{\mathbf{B}} = 0, \quad (2.25)$$

where the mean Lorentz force is $\bar{\mathbf{F}}_L = \bar{\mathbf{B}} \cdot \bar{\nabla} \bar{\mathbf{B}} + \overline{\mathbf{b}' \cdot \nabla \mathbf{b}'}$.

The fluctuating equations are found by subtracting the mean equations from the full equations to give

$$\begin{aligned} \left(\partial_t + \frac{1}{A_\tau}\partial_\tau + \frac{1}{A_T}\partial_T\right)\mathbf{u}' + \bar{\mathbf{u}} \cdot \nabla \mathbf{u}' + \mathbf{u}' \cdot \bar{\nabla} \bar{\mathbf{u}} - \bar{\nabla} \cdot (\overline{\mathbf{u}'(\mathbf{u}')^{tr}}) + \frac{1}{Ro}\hat{\mathbf{z}} \times \mathbf{u}' = \\ -Eu(\bar{\nabla} + \nabla)p' + M\mathbf{F}'_L + \Gamma\theta'\hat{\mathbf{z}} + \frac{1}{Re}(\nabla^2 + \bar{\nabla}^2)\mathbf{u}', \end{aligned} \quad (2.26)$$

$$\begin{aligned} \left(\partial_t + \frac{1}{A_\tau}\partial_\tau + \frac{1}{A_T}\partial_T\right)\theta' + \mathbf{u}' \cdot \bar{\nabla} \bar{\theta} + \bar{\mathbf{u}} \cdot \nabla \theta' + \bar{\nabla} \cdot (\mathbf{u}'\theta') - \bar{\nabla} \cdot (\overline{\mathbf{u}'\theta'}) = \\ \frac{1}{Pe}(\nabla^2 + \bar{\nabla}^2)\theta', \end{aligned} \quad (2.27)$$

$$\begin{aligned} \left(\partial_t + \frac{1}{A_\tau}\partial_\tau + \frac{1}{A_T}\partial_T\right)\mathbf{b}' = \\ \bar{\nabla} \times (\bar{\mathbf{u}} \times \mathbf{b}') + \bar{\nabla} \times (\mathbf{u}' \times \bar{\mathbf{B}}) + \bar{\nabla} \times (\mathbf{u}' \times \mathbf{b}') - \bar{\nabla} \times (\overline{\mathbf{u}' \times \mathbf{b}'}) + \\ \nabla \times (\bar{\mathbf{u}} \times \mathbf{b}') + \nabla \times (\mathbf{u}' \times \bar{\mathbf{B}}) + \nabla \times (\mathbf{u}' \times \mathbf{b}') + \frac{1}{Rm}(\nabla^2 + \bar{\nabla}^2)\mathbf{b}', \\ (\bar{\nabla} + \nabla) \cdot \mathbf{u}' = 0, \quad (\bar{\nabla} + \nabla) \cdot \mathbf{b}' = 0, \end{aligned} \quad (2.28)$$

where the fluctuating Lorentz force is $\mathbf{F}'_L = \bar{\mathbf{B}} \cdot \nabla \mathbf{b}' + \mathbf{b}' \cdot \bar{\nabla} \bar{\mathbf{B}} + \mathbf{b}' \cdot \nabla \mathbf{b}' - \overline{\mathbf{b}' \cdot \nabla \mathbf{b}'}$.

2.2. Asymptotics

We note that up to this point, no approximations have been made; the equations have simply been split up into mean and fluctuating components. In the present work we are interested in the development of a multiscale dynamo model that preserves geostrophic balance on the small (fluctuating) scales. Because the fluctuating and mean dynamics are coupled, *a posteriori* we find that the large-scales are required to also be geostrophically balanced in the horizontal directions, and hydrostatic in the vertical direction, resulting in a thermal wind balance. The relevant asymptotic limit for the present model is therefore the small-Rossby number limit, $Ro \equiv \epsilon \rightarrow 0$.

When constructing an asymptotic model with more than one small (or large) parameter, it is necessary to establish the so-called distinguished limits, or the asymptotic scaling relationships between the various parameters. In the present context this implies that we must relate, in an order of magnitude sense, both the non-dimensional parameters introduced in equations (2.5)-(2.6), as well as the aspect ratios defined by equations (2.17), to the Rossby number ϵ . This procedure is well known, and hinges on the identification of dominant balances in the governing equations that will allow for a mathematically and physically meaningful reduced model; by definition the procedure is circular in nature (e.g. see Bender & Orszag 2010). In this regard, to ensure geostrophically balanced convection on the small scales, we follow section 2 of Sprague *et al.* (2006) and employ the following distinguished limits

$$A_Z = \epsilon^{-1}, \quad A_T = \epsilon^{-2}, \quad Eu = \epsilon^{-2}, \quad \Gamma = \epsilon^{-1}\tilde{\Gamma}, \quad Re = O(1), \quad Pe = O(1). \quad (2.30)$$

We note that with these scalings, the small-scale velocity field \mathbf{u}' is $O(1)$, and we further assume the large-scale magnetic field $\bar{\mathbf{B}}$ to also be $O(1)$.

It then remains to determine the distinguished limits of A_X , A_τ , M , and Rm . To provide some explanation as to how these limits are achieved we examine various terms in the governing equations that we wish to retain in the final reduced model. The distinguished limit of A_X can be determined by restricting the large-scale horizontal motions to be geostrophically balanced; utilizing equation (2.22) we have

$$\frac{1}{\epsilon} \hat{\mathbf{z}} \times \bar{\mathbf{u}} \approx -\frac{1}{\epsilon^2 A_X} \nabla_X \bar{p}, \quad (2.31)$$

where $\nabla_X = (\partial_X, \partial_Y, 0)$. We then get

$$\bar{\mathbf{u}} \sim (\epsilon A_X)^{-1}, \quad (2.32)$$

where we have assumed $\bar{p} = O(1)$. Turning our attention to the mean temperature equation (2.23), we wish to keep horizontal advection of the mean temperature by the mean velocity field at the same order as the temporal evolution of the mean temperature so that

$$\epsilon^2 \partial_T \bar{\theta} \sim \frac{1}{A_X} \bar{\mathbf{u}} \cdot \nabla_X \bar{\theta}, \quad (2.33)$$

which leads to

$$\bar{\mathbf{u}} \sim \epsilon^2 A_X. \quad (2.34)$$

Combining (2.32) with (2.34) then shows that we must have

$$A_X = \epsilon^{-3/2}, \quad (2.35)$$

and so $\bar{\mathbf{u}} = O(\epsilon^{1/2})$.

The distinguished limits of A_τ , M , and Rm are determined by examining the influence of the magnetic field. To generate dynamo action on the large scales via coupling with the fluctuating dynamics, we necessarily require the presence of the second term on the righthand side of (2.24), where $(\bar{\mathbf{u}}' \times \mathbf{b}')$ is referred to as the mean electromotive force, or mean emf (e.g. Parker 1955; Steenbeck *et al.* 1966; Steenbeck & Krause 1966; Moffatt 1978). Utilizing the above scalings for A_X and $\bar{\mathbf{u}}$, and retaining only the largest terms, the order of magnitude of each term present in the mean induction equation is then

$$\frac{\bar{\mathbf{B}}}{A_\tau} : \epsilon^{3/2} \bar{\mathbf{B}} : \epsilon \mathbf{b}' : \frac{\epsilon^2}{Rm} \bar{\mathbf{B}}, \quad (2.36)$$

where we recall that the fluctuating velocity field is order one, consistent with Sprague *et al.* (2006). To retain time dependence of the mean magnetic field, we require that the first and third terms be of the same magnitude such that

$$\bar{\mathbf{B}} \sim \epsilon A_\tau \mathbf{b}'. \quad (2.37)$$

By noting that all the large-scale gradients are small relative to the small-scale gradients, the order of magnitude of the four largest terms (the first on the lefthand side, and the fifth, sixth and eighth terms on the righthand side) in the fluctuating induction equation (2.28) are

$$\mathbf{b}' : \bar{\mathbf{B}} : \mathbf{b}' : \frac{\mathbf{b}'}{Rm}. \quad (2.38)$$

We require that ohmic dissipation is present in the final model, at least with respect to the small scales. The largest term present above would then be that associated with

stretching the mean magnetic field such that

$$\overline{\mathbf{B}} \sim \frac{\mathbf{b}'}{Rm}. \quad (2.39)$$

Finally, because we're investigating dynamo action, we require that the Lorentz force enter the small scale momentum dynamics. From Sprague *et al.* (2006), and examination of equation (2.26) we know that this requires

$$M\overline{\mathbf{B}}\mathbf{b}' = O(1). \quad (2.40)$$

Combining this scaling with (2.39) yields

$$M = O(Rm^{-1}), \quad (2.41)$$

recalling that $\overline{\mathbf{B}}$ is order one. We can now determine the size of Rm by returning to the mean induction equation; by balancing the mean emf with magnetic diffusion (the third and fourth terms, respectively, given in (2.36)) we have

$$\epsilon\mathbf{b}' \sim \frac{\epsilon^2}{Rm}\overline{\mathbf{B}}. \quad (2.42)$$

Using the above scaling with (2.39) shows that

$$Rm \geq \epsilon^{1/2}, \quad (2.43)$$

with the lower bound being the case $Rm = \epsilon^{1/2}$. The particular distinguished limit taken for Rm will in turn determine the size of the magnetic Prandtl number since $Rm = RePm$. Taking $Rm = \epsilon^{1/2}$ corresponds to the low Pm limit since $Re = O(1)$. An alternative scaling would be to take $Rm = O(1)$ and thus $Pm = O(1)$. The main focus of the present manuscript is for the $Rm = \epsilon^{1/2}$ limit given that it ties directly to the CSDM and is implicitly low Pm . We also present the form of the governing equations for the $Rm = O(1)$, but note additional complications that arise in this limit which will require analysis in the future.

2.2.1. The $Rm = \epsilon^{1/2}$ Limit

Taking $Rm = \epsilon^{1/2}$ and returning to relationships (2.37) and (2.41) we can now define the distinguished limits of A_τ and M as

$$A_\tau = \epsilon^{-3/2}, \quad M = \epsilon^{-1/2}, \quad (2.44)$$

showing that three disparate timescales are now present in the QGDM.

With our distinguished limits defined, we now follow CS72 and expand all variables in powers of $\epsilon^{1/2}$, e.g.

$$\mathbf{u}' = \mathbf{u}'_0 + \epsilon^{1/2}\mathbf{u}'_{1/2} + \epsilon\mathbf{u}'_1 + \dots \quad (2.45)$$

Plugging the perturbation expansions into the governing equations and collecting terms of equal magnitude, the leading order solenoidal conditions on the mean velocity and magnetic fields gives

$$\partial_Z \overline{w}_0 = 0, \quad \partial_Z \overline{D}_0 = 0. \quad (2.46)$$

Owing to our use of impenetrable, perfectly conducting boundary conditions we require $\overline{w}_0 = \overline{D}_0 = 0$. At the next order the solenoidal conditions yield

$$\nabla_X \cdot \overline{\mathbf{u}}_0 + \partial_Z \overline{w}_{1/2} = 0, \quad \nabla_X \cdot \overline{\mathbf{B}}_0 + \partial_Z \overline{D}_{1/2} = 0. \quad (2.47)$$

At order $\mathcal{O}(\epsilon^{-1})$ the horizontal mean momentum equation gives

$$\widehat{\mathbf{z}} \times \overline{\mathbf{u}}_0 = 0, \quad (2.48)$$

showing that $\bar{\mathbf{u}}_0 \equiv 0$. Utilizing continuity it follows that $\bar{w}_{1/2} \equiv 0$. The next three orders of the mean horizontal momentum equation are then geostrophically balanced,

$$\hat{\mathbf{z}} \times \bar{\mathbf{u}}_i = -\nabla_X \bar{p}_{i-1/2}, \quad i = \frac{1}{2}, 1, \frac{3}{2}. \quad (2.49)$$

Carrying the expansion out to $O(\epsilon)$ shows that $\bar{\mathbf{u}}_2$ is magnetostrophically balanced,

$$\hat{\mathbf{z}} \times \bar{\mathbf{u}}_2 = -\nabla_X \bar{p}_{3/2} + \bar{\mathbf{B}}_0 \cdot \nabla_X \bar{\mathbf{B}}_0 + \bar{D}_{1/2} \partial_Z \bar{\mathbf{B}}_0. \quad (2.50)$$

The vertical mean momentum equation yields hydrostatic balance for the first four orders,

$$\partial_Z \bar{p}_i = \tilde{\Gamma} \bar{\theta}_i, \quad i = 0, \frac{1}{2}, 1, \frac{3}{2}. \quad (2.51)$$

We assume that contributions from a vertically averaged, barotropic mode are identically zero given that the evolution equation for such a mode enters at a much higher, subdominant order (c.f. Dolapchiev & Klein 2009). Taking the curl of equation (2.49) with $i = 1/2$ shows that $\nabla_X \cdot \bar{\mathbf{u}}_{1/2} = 0$, and thus $\bar{w}_1 \equiv 0$. Combining equation (2.49) with $i = 1/2$ and (2.51) with $i = 0$ we then obtain the well-known thermal wind relations

$$\partial_Z \bar{v}_{1/2} = \tilde{\Gamma} \partial_X \bar{\theta}_0, \quad \partial_Z \bar{u}_{1/2} = -\tilde{\Gamma} \partial_Y \bar{\theta}_0. \quad (2.52)$$

Because the large-scale velocity field is horizontally divergence free we can define the large-scale geostrophic stream function as $\bar{\Psi}_0 \equiv \bar{p}_0$ such that

$$\bar{\mathbf{u}}_{1/2} = -\bar{\nabla} \times \bar{\Psi}_0 \hat{\mathbf{z}}. \quad (2.53)$$

Proceeding to the mean horizontal induction equation, at $O(\epsilon)$ we have

$$0 = \partial_Z \left[\hat{\mathbf{z}} \times \overline{(\mathbf{u}'_0 \times \mathbf{b}'_0)} \right], \quad (2.54)$$

which, in general, requires that $\mathbf{b}'_0 \equiv 0$. Alternatively, from the scaling relationship given by (2.39), we require that $\mathbf{b}' = O(\epsilon^{1/2})$ if $\bar{\mathbf{B}} = O(1)$. At $O(\epsilon^{3/2})$ we get

$$\partial_\tau \bar{\mathbf{B}}_0^\perp = \partial_Z \left[\hat{\mathbf{z}} \times \overline{(\mathbf{u}'_0 \times \mathbf{b}'_{1/2})} \right] + \partial_Z^2 \bar{\mathbf{B}}_0^\perp, \quad (2.55)$$

where $\bar{\mathbf{B}}_0^\perp \equiv (\bar{B}_0, \bar{C}_0, 0)$. The leading order vertical component of the induction equation becomes

$$\partial_\tau \bar{D}_{1/2} = \partial_X \left[\hat{\mathbf{y}} \cdot \overline{(\mathbf{u}'_0 \times \mathbf{b}'_{1/2})} \right] - \partial_Y \left[\hat{\mathbf{x}} \cdot \overline{(\mathbf{u}'_0 \times \mathbf{b}'_{1/2})} \right] + \partial_Z^2 \bar{D}_{1/2}, \quad (2.56)$$

where we see that a non-trivial mean vertical magnetic field requires the presence of a large-scale horizontal modulation. The fluctuating induction equation then gives

$$0 = \bar{\mathbf{B}}_0^\perp \cdot \nabla_\perp \mathbf{u}'_0 + \nabla_\perp^2 \mathbf{b}'_{1/2}, \quad (2.57)$$

which is identical to the small-scale induction equation first derived by S74.

The leading order mean temperature equation gives

$$\partial_Z \overline{(w'_0 \theta'_0)} = 0, \quad (2.58)$$

showing that $\theta'_0 \equiv 0$. At the next order we have

$$\partial_\tau \bar{\theta}_0 + \partial_Z \overline{(w'_0 \theta'_{1/2})} = 0, \quad (2.59)$$

again showing that $\theta'_{1/2} \equiv 0$ and thus $\partial_\tau \bar{\theta}_0 \equiv 0$. Finally, we have

$$\partial_\tau \bar{\theta}_{1/2} + \partial_T \bar{\theta}_0 + \bar{\mathbf{u}}_{1/2} \cdot \nabla_X \bar{\theta}_0 + \partial_Z \overline{(w'_0 \theta'_1)} = \frac{1}{Pe} \partial_Z^2 \bar{\theta}_0. \quad (2.60)$$

To avoid secular growth of the mean temperature on the timescale τ we must have $\partial_\tau \bar{\theta}_{1/2} \equiv 0$; the mean heat equation then becomes

$$\partial_T \bar{\theta}_0 + \bar{\mathbf{u}}_{1/2} \cdot \nabla_X \bar{\theta}_0 + \partial_Z \overline{(w'_0 \theta'_1)} = \frac{1}{Pe} \partial_Z^2 \bar{\theta}_0. \quad (2.61)$$

Alternatively, one can average equation (2.60) over the timescale τ to obtain an equation identical to (2.61), with the exception that the averages must then be interpreted as occurring over (\mathbf{x}, t, τ) . At $O(\epsilon)$ the fluctuating temperature equation is

$$\partial_t \theta'_1 + \mathbf{u}'_0 \cdot \nabla_\perp \theta'_1 + w'_0 \partial_Z \bar{\theta}_0 = \frac{1}{Pe} \nabla_\perp^2 \theta'_1. \quad (2.62)$$

At $O(\epsilon^{-2})$ and $O(\epsilon^{-3/2})$ the fluctuating momentum equation yields, respectively

$$\nabla p'_i = 0, \quad i = 0, \frac{1}{2}, \quad (2.63)$$

showing that $p'_0 = p'_{1/2} \equiv 0$. Geostrophy occurs at $O(\epsilon^{-1})$ and $O(\epsilon^{-1/2})$

$$\hat{\mathbf{z}} \times \mathbf{u}'_i = -\nabla p'_{i+1}, \quad i = 0, \frac{1}{2}. \quad (2.64)$$

Additionally, mass conservation at $O(1)$ and $O(\epsilon^{1/2})$ gives

$$\nabla \cdot \mathbf{u}'_i = 0, \quad i = 0, \frac{1}{2}, \quad (2.65)$$

which, along with equations (2.64), yields the Proudman-Taylor theorem acting over the small vertical scale z

$$\partial_z (\mathbf{u}'_i, p'_{i+1}) = 0, \quad i = 0, \frac{1}{2}. \quad (2.66)$$

The prognostic momentum equation then appears at $O(1)$

$$\partial_t \mathbf{u}'_0 + \mathbf{u}'_0 \cdot \nabla_\perp \mathbf{u}'_0 + \hat{\mathbf{z}} \times \mathbf{u}'_1 = -\nabla p'_2 - \partial_Z p'_1 \hat{\mathbf{z}} + \tilde{\Gamma} \theta'_1 \hat{\mathbf{z}} + \bar{\mathbf{B}}_0 \cdot \nabla_\perp \mathbf{b}'_{1/2} + \frac{1}{Re} \nabla_\perp^2 \mathbf{u}'_0, \quad (2.67)$$

where we note the key distinction with the CSDM is the simultaneous appearance of both the advection and Lorentz force terms. In light of equation (2.64), we can define the small-scale geostrophic stream function as $\psi_0 \equiv p'_1$ such that the fluctuating horizontal velocity field is given by $(u'_0, v'_0) = (-\partial_y \psi_0, \partial_x \psi_0)$. Following Sprague *et al.* (2006), solvability is obtained by taking $\hat{\mathbf{z}} \cdot \nabla \times$ and $\hat{\mathbf{z}} \cdot$ the above equation and averaging over the small vertical scale z to obtain

$$\partial_t \nabla_\perp^2 \psi_0 + J(\psi_0, \nabla_\perp^2 \psi_0) - \partial_Z w'_0 = \hat{\mathbf{z}} \cdot \nabla \times \left(\bar{\mathbf{B}}_0 \cdot \nabla_\perp \langle \mathbf{b}'_{1/2} \rangle \right) + \frac{1}{Re} \nabla_\perp^4 \psi_0, \quad (2.68)$$

$$\partial_t w'_0 + J(\psi_0, w'_0) + \partial_Z \psi_0 = \tilde{\Gamma} \theta'_1 + \hat{\mathbf{z}} \cdot \left(\bar{\mathbf{B}}_0 \cdot \nabla_\perp \langle \mathbf{b}'_{1/2} \rangle \right) + \frac{1}{Re} \nabla_\perp^2 w'_0, \quad (2.69)$$

where $J(F, G) = \partial_x F \partial_y G - \partial_x G \partial_y F$, the angled brackets denote a spatial average over z , and the vertical vorticity is $\zeta_0 = \nabla_\perp^2 \psi_0$.

Upon rescaling the velocity with the small-scale viscous diffusion time such that $U =$

ν/L , the closed set of reduced equations is given by

$$\bar{\mathbf{u}}_{1/2} = -\bar{\nabla} \times \bar{\Psi}_0 \hat{\mathbf{z}}, \quad (2.70)$$

$$\partial_Z \bar{\Psi}_0 = \frac{\widetilde{Ra}}{Pr} \bar{\theta}_0, \quad (2.71)$$

$$\partial_T \bar{\theta}_0 + \bar{\mathbf{u}}_{1/2} \cdot \nabla_X \bar{\theta}_0 + \partial_Z \overline{(w'_0 \theta'_1)} = \frac{1}{Pr} \partial_Z^2 \bar{\theta}_0, \quad (2.72)$$

$$\partial_\tau \bar{\mathbf{B}}_0^\perp = \partial_Z \left[\hat{\mathbf{z}} \times \overline{(\mathbf{u}'_0 \times \langle \mathbf{b}'_{1/2} \rangle)} \right] + \partial_Z^2 \bar{\mathbf{B}}_0^\perp, \quad (2.73)$$

$$\partial_\tau \bar{D}_{1/2} = \partial_X \left[\hat{\mathbf{y}} \cdot \overline{(\mathbf{u}'_0 \times \langle \mathbf{b}'_{1/2} \rangle)} \right] - \partial_Y \left[\hat{\mathbf{x}} \cdot \overline{(\mathbf{u}'_0 \times \langle \mathbf{b}'_{1/2} \rangle)} \right] + \partial_Z^2 \bar{D}_{1/2}, \quad (2.74)$$

$$\partial_X \bar{B}_0 + \partial_Y \bar{C}_0 + \partial_Z \bar{D}_{1/2} = 0, \quad (2.75)$$

$$\partial_t \nabla_\perp^2 \psi_0 + J(\psi_0, \nabla_\perp^2 \psi_0) - \partial_Z w'_0 = \hat{\mathbf{z}} \cdot \nabla \times \left(\bar{\mathbf{B}}_0 \cdot \nabla_\perp \langle \mathbf{b}'_{1/2} \rangle \right) + \nabla_\perp^4 \psi_0, \quad (2.76)$$

$$\partial_t w'_0 + J(\psi_0, w'_0) + \partial_Z \psi_0 = \frac{\widetilde{Ra}}{Pr} \theta'_1 + \bar{\mathbf{B}}_0 \cdot \nabla_\perp \langle d'_{1/2} \rangle + \nabla_\perp^2 w'_0, \quad (2.77)$$

$$\partial_t \theta'_1 + J(\psi_0, \theta'_1) + w'_0 \partial_Z \bar{\theta}_0 = \frac{1}{Pr} \nabla_\perp^2 \theta'_1, \quad (2.78)$$

$$0 = \bar{\mathbf{B}}_0^\perp \cdot \nabla_\perp \mathbf{u}'_0 + \nabla_\perp^2 \langle \mathbf{b}'_{1/2} \rangle, \quad (2.79)$$

$$\partial_x \langle b'_{1/2} \rangle + \partial_y \langle c'_{1/2} \rangle = 0. \quad (2.80)$$

The reduced Rayleigh number, consistent with the linear theory of rapidly rotating convection (Chandrasekhar 1961), is defined by $\widetilde{Ra} = \epsilon^4 Ra_H = E_H^{4/3} Ra_H$, where the Rayleigh number is given by

$$Ra_H = \frac{g \alpha \Delta T H^3}{\nu \kappa}. \quad (2.81)$$

Written in terms of the reduced variables the boundary conditions become

$$\bar{\theta}_0 = 1 \quad \text{at} \quad Z = 0, \quad \bar{\theta}_0 = 0 \quad \text{at} \quad Z = 1, \quad (2.82)$$

$$\partial_Z \bar{\mathbf{B}}_0^\perp = \bar{D}_{1/2} = w'_0 = 0 \quad \text{at} \quad Z = 0, 1. \quad (2.83)$$

2.2.2. The $Rm = O(1)$ Limit

The asymptotic development of the $Rm = O(1)$ parallels that for the $Rm = \epsilon^{1/2}$ case given above. For this reason we omit many of the details and focus only on the differences between the two limiting cases. We emphasize again that the $Rm = O(1)$ limit corresponds to $Pm = O(1)$ since $Re = O(1)$. Consideration of relationships (2.37) and (2.41) with $Rm = O(1)$ shows that we must have

$$A_\tau = \epsilon^{-1}, \quad M = O(1). \quad (2.84)$$

In addition, relationship (2.39) shows that the mean and fluctuating magnetic fields are now of the same order, i.e. $\bar{\mathbf{B}} \sim \mathbf{b}'$. The main difference that occurs in the final reduced model for the $Rm = O(1)$ case is the form of the induction equations, which at leading

order become

$$\partial_\tau \overline{\mathbf{B}}_0^\perp = \partial_Z \left[\widehat{\mathbf{z}} \times \overline{(\mathbf{u}'_0 \times \langle \mathbf{b}'_0 \rangle)} \right], \quad (2.85)$$

$$\partial_\tau \overline{D}_{1/2} = \partial_X \left[\widehat{\mathbf{y}} \cdot \overline{(\mathbf{u}'_0 \times \langle \mathbf{b}'_0 \rangle)} \right] - \partial_Y \left[\widehat{\mathbf{x}} \cdot \overline{(\mathbf{u}'_0 \times \langle \mathbf{b}'_0 \rangle)} \right], \quad (2.86)$$

$$\partial_t \langle \mathbf{b}'_0 \rangle + \mathbf{u}'_0 \cdot \nabla_\perp \langle \mathbf{b}'_0 \rangle = \overline{\mathbf{B}}_0^\perp \cdot \nabla_\perp \mathbf{u}'_0 + \frac{1}{Pm} \nabla_\perp^2 \langle \mathbf{b}'_0 \rangle. \quad (2.87)$$

The fluctuating equations then take a mathematically equivalent form of equations (2.76)-(2.78) and (2.80) by making the substitution $\langle \mathbf{b}'_{1/2} \rangle \rightarrow \langle \mathbf{b}'_0 \rangle$.

The boundary conditions for the $Rm = O(1)$ case are identical to those given by (2.82)-(2.83). Equations (2.85)-(2.86) shows that owing to the absence of Z -derivatives, the mean magnetic field boundary conditions can no longer be satisfied without the inclusion of magnetic boundary layers. Future work is necessary to examine the effects of these boundary layers.

3. Discussion

3.1. The $Rm = \epsilon^{1/2}$ Limit

Here we reiterate some of the key features of the low magnetic Prandtl number QGDM and interpret the various terms in the equation set (2.70)-(2.80). Equations (2.70)-(2.71) are statements of geostrophic balance and hydrostatic balance on the large horizontal and vertical scales, respectively. Importantly, these equations are diagnostic since they contain no information about the temporal evolution; this is a well-known characteristic and the prognostic dynamics are obtained from the mean heat equation (2.72). From equation (2.70) we see that viscous diffusion is negligible on the large scales. The mean heat equation given by (2.72) shows that the mean velocity field is strong enough to allow advection of the mean temperature over the large horizontal scales (X, Y) as shown by the second term on the lefthand side, whereas the third term represents the influence of convective feedback from the fluctuating scales back onto the large-scales. Additionally, the presence of large-scale thermal diffusion over the vertical dimension is represented by the term on the righthand side of equation (2.72).

Both of the mean induction equations given by (2.73) and (2.74) contain time dependence, the mean emf that represents the feedback from fluctuating velocity and magnetic field dynamics, and ohmic diffusion on the large vertical scale Z . Thus, ohmic dissipation dominates viscous dissipation on the large scales since, at this order of approximation, viscous diffusion is not present in equations (2.70)-(2.71). This feature is consistent with the $Pm \ll 1$ limit considered here. Moreover, the QGDM is characterized by a horizontal magnetic field that is $O(Rm)$ stronger than the vertical magnetic field.

Equations (2.76)-(2.78) are a magnetic version of the quasi-geostrophic convection equations originally developed by Sprague *et al.* (2006). An important feature of equations (2.76)-(2.77) is that both advection and diffusion only occur over the small horizontal scales (x, y) due to the anisotropic spatial structure of low Rossby number convection. The fluctuating vorticity equation (2.76) contains time dependence, advection on the small-scales, vortex stretching is represented by the third term on the lefthand side, with the remaining terms on the righthand side being the Lorentz force and viscous diffusion, respectively. The fluctuating momentum equation is given by (2.77) and, like the fluctuating vorticity equation, contains time dependence and horizontal advection. The vertical pressure gradient is given by the third term on the lefthand side of equation (2.77), with the fluctuating geostrophic stream function ψ_0 acting as pressure since

the flow is geostrophically balanced; the remaining terms on the righthand side are the buoyancy force, the Lorentz force, and viscous diffusion. The fluctuating heat equation (2.78) is also characterized by time dependence and horizontal advection and diffusion, with the third term on the lefthand side representing advection of the mean heat by the fluctuating vertical velocity over the large-scale Z .

The fluctuating induction equation (2.79) is identical to the equation given in S74, where he noted that the fluctuating magnetic field is induced by stretching the mean magnetic field with the small-scale strain $\nabla_{\perp} \mathbf{u}'_0$ (consistent with our low Rm approximation). The absence of the time derivative shows that the fluctuating magnetic field adjusts instantaneously relative to the fluctuating convection, showing that magnetic diffusion is much more rapid than momentum diffusion on the small-scales; this effect is consistent with a small magnetic Prandtl number limit. As with the fluctuating vorticity, momentum, and heat equations, only horizontal diffusion is present in the fluctuating induction owing to spatial anisotropy. Taken with equations (2.76)-(2.78), we see that both viscous dissipation and ohmic dissipation are important features for the small-scale dynamics. The small-scale induction equation also shows that both the present model and the CSDM require the presence of a non-trivial mean magnetic field for the development of a dynamo; this shows that the resulting dynamo is therefore large-scale and typical of low Rm dynamos.

In the present work three timescales were necessary to allow time variations of the fluctuating convection, the mean magnetic field, and the mean temperature. The relative ordering of these timescales is given by

$$t \ll A_{\tau}\tau \ll A_T T, \quad (3.1)$$

or

$$t \ll \epsilon^{-3/2}\tau \ll \epsilon^{-2}T, \quad (3.2)$$

upon noting that $\tau = A_{\tau}^{-1}t$ and $T = A_T^{-1}t$. This ordering states that the large-scale magnetic diffusion timescale lies midway between the small-scale convective timescale and the large-scale thermal diffusion timescale. For the geodynamo, observations of the geomagnetic field show that $t \sim O(1)$ year, $\tau \sim O(10^4)$ years and $T \sim O(10^9)$ years, suggesting that the above ordering is realistic.

Many of the distinguished limits that were taken in the present work can be related to values that we expect for the geodynamo. Utilizing the velocity based on the small-scale viscous diffusion timescale, the (small-scale) Rossby number can be related to the large-scale Ekman number as

$$\epsilon = Ro = E_H^{1/3}. \quad (3.3)$$

Studies suggest that the viscosity of the Earth's core is similar to that of water at standard temperature and pressure (e.g. Pozzo *et al.* 2013) such that $E_H \sim O(10^{-15})$. With this value we can obtain various estimates for other dimensionless parameters to test whether these are in general agreement with estimates based on observations; this exercise is useful for establishing the benefits and limitations of the present model. Estimates for the Rossby number, and the large-scale magnetic and hydrodynamic Reynolds numbers are given by, respectively,

$$\epsilon = 10^{-5}, \quad (3.4)$$

$$Rm_H = Rm E_H^{-1/3} = \epsilon^{-1/2} \sim O(10^2), \quad (3.5)$$

$$Re_H = Re E_H^{-1/3} = 10^5 Re. \quad (3.6)$$

The above estimate for the Rossby number is not too different from estimates based on

observations (Finlay & Amit 2011). The large-scale magnetic Reynolds number possesses the correct order of magnitude estimate for the core. For the large-scale Reynolds number Re_H we require knowledge of the currently unknown small-scale Reynolds number Re . Numerical simulations of the non-magnetic quasi-geostrophic convection equations can currently attain values of $Re \lesssim O(10^3)$ (e.g. Julien *et al.* 2012b), leading to large-scale Reynolds numbers of $Re_H \sim 10^8$; this suggests the QGDM is in the appropriate dynamical regime necessary for understanding the geodynamo.

The current model assumes an order one small-scale Reynolds number; coupled with the relationship $Rm = RePm$, this implies that $Pm = O(\epsilon^{1/2})$. The magnetic Prandtl number in the Earth’s core is thought to be $Pm \sim O(10^{-6})$, so it would seem that the distinguished limit taken for Pm is not quite in line with what typical values are in the Earth’s core. However, this may also imply that the limit $Pm = \epsilon^{1/2}$ may be sufficiently small to be in the asymptotic limit of small magnetic Prandtl number. Furthermore, the distinguished limit of $M = \epsilon^{-1/2}$ shows that magnetic energy dominates when $Pm \ll 1$; this result is thought to be consistent with what is known about the geodynamo.

3.2. The $Rm = O(1)$ Limit

The $Rm = O(1)$ case is associated with an order one magnetic Prandtl number. For this reason, the $Pm = O(1)$ QGDM may be particularly important for relating to DNS studies where reducing Pm to physically realistic values is impossible given the modest Reynolds numbers attainable with current computational resources. Given that the energy and momentum equations are identical to the low Pm QGDM discussed in the previous section, we focus here on the differences associated with the form of the induction equations (2.85)-(2.87).

The distinguished limit $A_\tau = \epsilon^{-1}$ shows that, in comparison to the $Rm = \epsilon^{1/2}$ case, the mean magnetic field now evolves on a faster timescale, though the timescale ordering given by relation (3.1) is preserved. The $M = O(1)$ limit indicates that the magnetic and kinetic energies are now equipartitioned when $Pm = O(1)$ – a result that appears to be consistent with DNS investigations (Stellmach & Hansen 2004).

The absence of Z -derivatives in equations (2.85)-(2.86) shows that ohmic dissipation is weak on the large-scales and limited to magnetic boundary layers adjacent to the horizontal boundaries. The small-scale induction equation (2.87) contains time dependence, advection by the fluctuating velocity field, along with stretching and diffusion. The presence of $\partial_t \langle \mathbf{b}'_0 \rangle$ results in a fluctuating magnetic field that no longer adjusts instantaneously to the fluctuating velocity field as it does when $Pm \ll 1$.

3.3. Relationship with the Childress-Soward Dynamo Model (CSDM)

In Table 1 we show the different distinguished limits taken between the present work and those taken by S74. Although we have considered two limits of Rm that result in different limits of M , Pm , and A_τ , the present discussion will be focused on the $Rm = \epsilon^{1/2}$ (low Pm) QGDM. The CSDM can be derived directly from equations (2.18)-(2.21) by employing the distinguished limits listed under the column labeled “Soward” and taking $\partial_t = \partial_T = \partial_X = \partial_Y \equiv 0$. The consequence of taking $Re = Pe = \epsilon^{1/2}$ is that the resulting model is weakly nonlinear since (horizontal) viscous diffusion enters at higher order than the advective nonlinearities in the fluctuating momentum equation. While in the present work we have considered both low and order one Pm , the CSDM employs $Pm = O(1)$. Additionally, the magnetic field scaling $M^S = \epsilon^{3/2}$ employed by S74 contrasts sharply with our $M = \epsilon^{-1/2}$ limit; the result is that magnetic energy is significantly larger than the kinetic energy in the present work.

It is possible to extend the CSDM to include fully nonlinear motions, a strong magnetic

Parameter	Present Work	Soward
Eu	ϵ^{-2}	ϵ^{-2}
Re	$O(1)$	$\epsilon^{1/2}$
M	$\epsilon^{-1/2}, O(1)$	$\epsilon^{3/2}$
Γ	$\tilde{\Gamma}\epsilon^{-1}$	$\tilde{\Gamma}\epsilon^{-1}$
Pe	$O(1)$	$\epsilon^{1/2}$
Rm	$\epsilon^{1/2}, O(1)$	$\epsilon^{1/2}$
Pr	$O(1)$	$O(1)$
Pm	$\epsilon^{1/2}, O(1)$	$O(1)$
A_X	$\epsilon^{-3/2}$	—
A_Z	ϵ^{-1}	ϵ^{-1}
A_τ	$\epsilon^{-3/2}$	$\epsilon^{-3/2}$
A_T	ϵ^{-2}	—

Table 1: Comparison between the different distinguished limits taken in the present work and those of Soward (1974), relative to equations (2.18)-(2.21). We note that Soward's model is weakly nonlinear and considers only a single (slow) timescale and a single large-scale coordinate in the governing equations such that $\partial_t = \partial_T = \partial_X = \partial_Y \equiv 0$. In both models the small parameter is the Rossby number, $Ro = \epsilon$, and $\tilde{\Gamma} = O(1)$.

field, and small Pm by neglecting the large-scale horizontal modulations (i.e. $\partial_X = \partial_Y = 0$) appearing in equations (2.71)-(2.80); the result is given by

$$\partial_Z \bar{\Psi}_0 = \frac{\widetilde{Ra}}{Pr} \bar{\theta}_0, \quad (3.7)$$

$$\partial_T \bar{\theta}_0 + \partial_Z \overline{(w'_0 \theta'_1)} = \frac{1}{Pr} \partial_Z^2 \bar{\theta}_0, \quad (3.8)$$

$$\partial_\tau \bar{\mathbf{B}}_0^\perp = \partial_Z \left[\hat{\mathbf{z}} \times \overline{(\mathbf{u}'_0 \times \langle \mathbf{b}'_{1/2} \rangle)} \right] + \partial_Z^2 \bar{\mathbf{B}}_0^\perp, \quad (3.9)$$

$$\partial_t \nabla_\perp^2 \psi_0 + J(\psi_0, \nabla_\perp^2 \psi_0) - \partial_Z w'_0 = \hat{\mathbf{z}} \cdot \nabla \times \left(\bar{\mathbf{B}}_0 \cdot \nabla_\perp \langle \mathbf{b}'_{1/2} \rangle \right) + \nabla_\perp^4 \psi_0, \quad (3.10)$$

$$\partial_t w'_0 + J(\psi_0, w'_0) + \partial_Z \psi_0 = \frac{\widetilde{Ra}}{Pr} \theta'_1 + \bar{\mathbf{B}}_0 \cdot \nabla_\perp \langle d'_{1/2} \rangle + \nabla_\perp^2 w'_0, \quad (3.11)$$

$$\partial_t \theta'_1 + J(\psi_0, \theta'_1) + w'_0 \partial_Z \bar{\theta}_0 = \frac{1}{Pr} \nabla_\perp^2 \theta'_1, \quad (3.12)$$

$$0 = \bar{\mathbf{B}}_0^\perp \cdot \nabla_\perp \mathbf{u}'_0 + \nabla_\perp^2 \langle \mathbf{b}'_{1/2} \rangle, \quad (3.13)$$

$$\partial_x \langle b'_{1/2} \rangle + \partial_y \langle c'_{1/2} \rangle = 0, \quad (3.14)$$

and we note that equaton (2.75) is trivially satisfied in this case.

CS72 described three different classes of dynamos, distinguished by the relative strength of the magnetic field. In their work, the classification was based on the magnitude of the large-scale Hartmann number defined as

$$Ha_H = \frac{\mathcal{B}H}{(\mu\rho\nu\eta)^{1/2}}. \quad (3.15)$$

In the CS72 terminology, the weak field, intermediate field, and strong field dynamos are characterized by Hartmann numbers of magnitude $Ha_H^w \sim O(1)$, $Ha_H^i \sim O(\epsilon^{-1/2})$ and $Ha_H^s \gg \epsilon^{-1/2}$, respectively. By employing our distinguished limits, the large-scale Hartmann number in the present work is given by

$$Ha_H^* = \frac{(MRm)^{1/2}}{\epsilon} = \frac{1}{\epsilon}. \quad (3.16)$$

Thus, by the classifications of CS72 the present model could be considered a strong field model. As the fluctuating momentum equation (2.67) shows, both the Lorentz force and horizontal viscous diffusion enter the prognostic equation at the same order in our model; the result is that the small-scale Hartmann number is unity, $Ha^* = 1$. In the S74 analysis, the Lorentz force enters at the same order as vertical viscous diffusion, leading to $Ha_H^S = 1$ in the CSDM.

In the wider literature, a strong field dynamo appears to be synonymous with the magnetostrophic balance. Our present model is geostrophically balanced on both the large and small scales, though as equation (2.50) shows a magnetostrophic balance does appear at higher, but subdominant, order in the mean momentum equation. A more appropriate dimensionless measure of the strong field dynamo is the Elsasser number, defined as the ratio of the Lorentz force to the Coriolis force and often expressed as

$$\Lambda = \frac{\mathcal{B}^2}{2\Omega\rho\mu\eta}. \quad (3.17)$$

In terms of the nondimensional parameters and distinguished limits employed in the present study (e.g. Table 1) we have

$$\Lambda = MPmRoRe = \epsilon. \quad (3.18)$$

Thus, as expected, the Elsasser number is small in our geostrophically balanced model. In S74 the Elsasser number is significantly smaller with $\Lambda^S = \epsilon^3$. Although DNS studies are often characterized by order one Elsasser number, we note that these models are all limited to $Pm \sim O(1)$ and moderate values of the Ekman number. We speculate that if these models could increase their magnetic Reynolds number solely by increasing their Reynolds number and decreasing the Ekman number, rather than increasing Pm , they would begin to reach significantly smaller Elsasser numbers; this trend may be apparent in the plane layer DNS investigation of Stellmach & Hansen (2004) and the spherical DNS study of Christensen & Aubert (2006). Also, we note that the value of the Elsasser number is also dependent upon how one scales the magnetic field. The form given by (3.17) is dependent upon the magnetic diffusivity since it is typically assumed that the magnitude of the current density scales as $\mathcal{J} \sim UB/\mu\eta$ (e.g. Davidson 2001). To be consistent, however, the Elsasser number should be defined directly from the governing equation as

$$\Lambda^* = \frac{\frac{1}{\rho\mu}\mathbf{B} \cdot \nabla \mathbf{B}}{2\Omega\hat{\mathbf{z}} \times \mathbf{u}} = \frac{\mathcal{B}^2}{2\Omega\rho\mu L\mathcal{U}} = MRo = \epsilon^{1/2}. \quad (3.19)$$

Similarly, for the $Rm = O(1)$ QGDM, this gives $\Lambda^* = \epsilon$. This shows that although the Elsasser number is still small, it is independent of the magnetic diffusivity. Given that the model developed in the present work is characterized by small Elsasser number, yet the magnetic energy is asymptotically larger than the kinetic energy for the low Pm QGDM, we can generally say that the partitioning of magnetic and kinetic energy is not necessarily indicative of dominant balances present within the governing equations.

4. Conclusion

In the present work we have utilized a standard multiple scales asymptotic approach to develop a new multiscale dynamo model that is valid in the limit of small Rossby, Ekman. The small-scale model is characterized by a magnetically-modified version of the quasi-geostrophic convection equations developed by Sprague *et al.* (2006). The large-scale model is characterized by a thermal wind balance in the mean momentum equations; coupled with the mean heat equation, the large-scale model is equivalent to the well-known planetary geostrophy equations commonly employed for investigating the dynamics of the Earth's atmosphere and ocean. We have discussed both low and order one magnetic Prandtl number models, showing that these two cases possess fundamentally different properties. For the low Pm case the magnetic energy dominates the kinetic energy, and ohmic dissipation is dominant over viscous dissipation on the large-scales. When $Pm = O(1)$ it was demonstrated that the magnetic and kinetic energies become equipartitioned with weak large-scale ohmic dissipation. The new model can be considered a fully nonlinear, generalized version of the so-called weak field dynamo model originally developed by Childress & Soward (1972).

Numerical simulations of asymptotically reduced equation sets have proven useful for accessing dynamical regimes in rotating plane layer convection that are computationally demanding or impossible to reach with the use of DNS (e.g. Sprague *et al.* 2006; Julien *et al.* 2012*a,b*; Rubio *et al.* 2014; Stellmach *et al.* 2014). These investigations have shown the dependence of the flow regime on both the Rayleigh and Prandtl numbers, new phenomena such as an asymptotic heat transfer scaling regime (Julien *et al.* 2012*a*), and large-scale vortex formation via an inverse cascade (Julien *et al.* 2012*b*). Numerical simulations of the new dynamo model will be important for investigating the influence of dynamo action on each of these phenomena.

Various extensions of the present work can also be carried out. While we have assumed, for simplicity, that the fluid is Boussinesq and that the gravity vector and rotation vector are aligned, it is a straightforward procedure to relax both of these constraints to include compressibility and varying angle between the gravity and rotation vectors (Julien *et al.* 2006; Mizerski & Tobias 2013). Although the anelastic approximation appears to agree well with the compressible equations for the case of order one Prandtl numbers (Calkins *et al.* 2014), it has recently been shown that it yields spurious results for low Prandtl number quasi-geostrophic convection (Calkins *et al.* 2015). However, Calkins *et al.* (2015) outlined an approach for extending the Boussinesq quasi-geostrophic convection equations of Sprague *et al.* (2006) to the case of a fully compressible gas. Moreover we believe that there are no technical issues to extending the current approach to rapidly rotating dynamos under the pseudo-incompressible approximation (Durrant 1989; Brown *et al.* 2012; Vasil *et al.* 2013).

The present model has focused on the plane layer geometry for the sake of mathematical and physical simplicity. To further the applicability of the present work with that of natural systems, it will be useful to extend the present methodology to the rotating cylindrical annulus (Busse 1986) and to spherical geometries. The three-dimensional cylindrical annulus model recently developed by Calkins *et al.* (2013) is particularly interesting since it possesses order one axial velocities, such that the Ekman pumping dynamo effect investigated by Busse (1975) is no longer a prerequisite for dynamo action in this geometry.

Observations indicate that the Rossby number for the largest scales in the Earth's outer core is $O(10^{-6})$. The Elsasser number for the large scale motions is $O(10^{-2})$, suggesting that the Lorentz force may not enter the leading order force balance for

the large-scale dynamics of the core (Nataf & Schaeffer 2015). Indeed, previous work calculating the angular momentum of the Earth’s outer core must invoke geostrophy to obtain the large-scale velocity field within the core, and shows excellent agreement with values obtained independently from observations of the Earth’s rotation rate (Jault *et al.* 1988; Jackson *et al.* 1993). These results suggest that the large-scale thermal wind model developed here may be relevant for understanding the geodynamo.

The small-scale dynamics of the geodynamo are completely unconstrained. The present work has utilized an expansion based on the smallness of the small-scale Rossby number. As discussed by Nataf & Schaeffer (2015), the precise value of the small-scale Rossby number depends upon the detailed properties of the turbulence that is controlled by the relative importance of inertia, buoyancy and the small-scale magnetic field. It may be that the Lorentz force increases in importance as the scale of motion decreases; again the precise nature of the importance of this interaction depends on the turbulence. Nataf & Schaeffer (2015) argue that although the Elsasser number is $O(0.01)$ for the largest scales of the Earth’s core, it increases to $O(1 - 10)$ on the scale of about 10km. Indeed, as the QGDM shows, if the Lorentz force is subdominant on the largest scales then it must be present in the small-scale dynamics to drive a dynamo. Future numerical simulations of the QGDM should therefore help to understand the small-scale dynamics of the geodynamo and other planetary magnetic fields (e.g. Stanley & Glatzmaier 2010).

Acknowledgements

This work was supported by the National Science Foundation under grants EAR #1320991 (MAC, KJ and JMA) and EAR CSEDI #1067944 (KJ and JMA).

REFERENCES

- BENDER, C. M. & ORSZAG, S. A. 2010 *Advanced mathematical methods for scientists and engineers I: Asymptotic methods and perturbation theory*. New York: Springer.
- BROWN, B. P., VASIL, G. M. & ZWEIBEL, E. G. 2012 Energy conservation and gravity waves in sound-proof treatments of stellar interiors. *Astrophys. J.* **756** (2).
- BUSSE, F. H. 1975 A model of the geodynamo. *Geophys. J. Roy. Astr. Soc.* **42**, 437–459.
- BUSSE, F. H. 1986 Asymptotic theory of convection in a rotating, cylindrical annulus. *J. Fluid Mech.* **173**, 545–556.
- CALKINS, M. A., JULIEN, K. & MARTI, P. 2013 Three-dimensional quasi-geostrophic convection in the rotating cylindrical annulus with steeply sloping endwalls. *J. Fluid Mech.* **732**, 214–244.
- CALKINS, M. A., JULIEN, K. & MARTI, P. 2014 Onset of rotating and non-rotating convection in compressible and anelastic ideal gases. *Geophys. Astrophys. Fluid Dyn.* **000**, 000.
- CALKINS, M. A., JULIEN, K. & MARTI, P. 2015 The breakdown of the anelastic approximation in rotating compressible convection: implications for astrophysical systems. *Proc. Roy. Soc. A* **000**, 000.
- CHANDRASEKHAR, S. 1961 *Hydrodynamic and Hydromagnetic Stability*. U.K.: Oxford University Press.
- CHARNEY, J. G. 1948 On the scale of atmospheric motions. *Geofys. Publ.* **17**, 3–17.
- CHILDRESS, S. & SOWARD, A. M. 1972 Convection-driven hydromagnetic dynamo. *Phys. Rev. Lett.* **29** (13), 837–839.
- CHRISTENSEN, U. & AUBERT, J. 2006 Scaling properties of convection-driven dynamos in rotating shells and applications to planetary magnetic fields. *Geophys. J. Int.* **166**, 97–114.
- DAVIDSON, P. A. 2001 *An Introduction to Magnetohydrodynamics*. Cambridge: Cambridge University Press.
- DOLAPTCHIEV, S. I. & KLEIN, R. 2009 Planetary geostrophic equations for the atmosphere with evolution of barotropic flow. *Dyn. Atmos. Oceans* **46**, 46–61.

- DURRAN, D. R. 1989 Improving the anelastic approximation. *J. Atmos. Sci.* **46** (11), 1453–1461.
- FAUTRELLE, Y. & CHILDRESS, S. 1982 Convective dynamos with intermediate and strong fields. *Geophys. Astrophys. Fluid Dyn.* **22** (3), 235–279.
- FAVIER, B. & PROCTOR, M. R. E. 2013 Kinematic dynamo action in square and hexagonal patterns. *Phys. Rev. E* **88** (053011).
- FINLAY, C. C. & AMIT, H. 2011 On flow magnitude and field-flow alignment at Earth’s core surface. *Geophys. J. Int.* **186**, 175–192.
- GROOMS, I., JULIEN, K. & FOX-KEMPER, B. 2011 On the interactions between planetary geostrophy and mesoscale eddies. *Dyn. Atmos. Oceans* **51**, 109–136.
- JACKSON, A., BLOXHAM, J. & GUBBINS, D. 1993 Time-dependent flow at the core surface and conservation of angular momentum in the coupled core-mantle system. *Dynamics of Earth’s Deep Interior and Earth Rotation* **72**, 97–107.
- JAULT, D., GIRE, C. & MOUËL, J. L. L. 1988 Westward drift, core motions and exchanges of angular momentum between core and mantle. *Nature* **333**, 353–356.
- JONES, C. A. 2011 Planetary magnetic fields and fluid dynamos. *Ann. Rev. Fluid Mech.* **43**, 583–614.
- JULIEN, K. & KNOBLOCH, E. 2007 Reduced models for fluid flows with strong constraints. *J. Math. Phys.* **48** (065405).
- JULIEN, K., KNOBLOCH, E., MILLIFF, R. & WERNE, J. 2006 Generalized quasi-geostrophy for spatially anisotropic rotationally constrained flows. *J. Fluid Mech.* **555**, 233–274.
- JULIEN, K., KNOBLOCH, E., RUBIO, A. M. & VASIL, G. M. 2012a Heat transport in Low-Rossby-number Rayleigh-Bénard Convection. *Phys. Rev. Lett.* **109** (254503).
- JULIEN, K., KNOBLOCH, E. & WERNE, J. 1998 A new class of equations for rotationally constrained flows. *Theoret. Comput. Fluid Dyn.* **11**, 251–261.
- JULIEN, K., RUBIO, A. M., GROOMS, I. & KNOBLOCH, E. 2012b Statistical and physical balances in low Rossby number Rayleigh-Bénard convection. *Geophys. Astrophys. Fluid Dyn.* **106** (4-5), 392–428.
- KING, E. M. & AURNOU, J. M. 2015 Magnetostrophic balance as the optimal state for turbulent magnetoconvection. *Proc. Nat. Acad. Sci.* **112** (4), 990–994.
- KING, E. M. & BUFFETT, B. A. 2013 Flow speeds and length scales in geodynamo models: the role of viscosity. *Earth Planet. Sci. Lett.* **371**, 156–162.
- KLEIN, R. 2010 Scale-dependent models for atmospheric flows. *Annu. Rev. Fluid Mech.* **42**, 249–274.
- MIESCH, M. S. 2005 Large-scale dynamics of the convection zone and tachocline. *Living Reviews in Solar Physics* **2** (1).
- MIZERSKI, K. A. & TOBIAS, S. M. 2013 Large-scale convective dynamos in a stratified rotating plane layer. *Geophys. Astrophys. Fluid Dyn.* **107** (1-2), 218–243.
- MOFFATT, H. K. 1978 *Magnetic Field Generation in Electrically Conducting Fluids*. Cambridge: Cambridge University Press.
- MOFFATT, H. K. 2008 Magnetostrophic turbulence and the geodynamo. In *IUTAM Symposium on Computational Physics and New Perspectives in Turbulence*, pp. 339–346. Springer.
- NATAF, H.-C. & SCHAEFFER, N. 2015 Turbulence in the core. In *Treatise on Geophysics* (ed. P. Olson & G. Schubert), , vol. 8. Elsevier.
- PARKER, E. N. 1955 Hydromagnetic dynamo models. *Astrophys. J.* **122**, 293–314.
- PEDLOSKY, J. 1987 *Geophysical Fluid Dynamics*. Springer-Verlag New York Inc.
- PHILLIPS, N. A. 1963 Geostrophic motion. *Rev. of Geophys.* **1** (2), 123–176.
- POZZO, M., DAVIES, C. J., GUBBINS, D. & ALFÉ, D. 2013 Transport properties for liquid silicon-oxygen-iron mixtures at Earth’s core conditions. *Phys. Rev. B* **87**, 014110.
- ROBERTS, P. H. 1988 Future of geodynamo theory. *Geophys. Astrophys. Fluid Dyn.* **44**, 3–31.
- ROBINSON, A. & STOMMEL, H. 1959 The oceanic thermocline and the associated thermohaline circulation. *Tellus* **11**, 295–308.
- RUBIO, A. M., JULIEN, K., KNOBLOCH, E. & WEISS, J. B. 2014 Upscale energy transfer in three-dimensional rapidly rotating turbulent convection. *Phys. Rev. Lett.* **112** (144501).
- SCHUBERT, G. & SODERLUND, K. 2011 Planetary magnetic fields: observations and models. *Phys. Earth Planet. Int.* **187**, 92–108.

- SODERLUND, K. M., KING, E. M. & AURNOU, J. M. 2012 The influence of magnetic fields in planetary dynamo models. *Earth Planet. Sci. Lett.* **333-334**, 9–20.
- SOWARD, A. M. 1974 A convection-drive dynamo: I. the weak field case. *Phil. Trans. R. Soc. Lond. A* **275**, 611–646.
- SPRAGUE, M., JULIEN, K., KNOBLOCH, E. & WERNE, J. 2006 Numerical simulation of an asymptotically reduced system for rotationally constrained convection. *J. Fluid Mech.* **551**, 141–174.
- STANLEY, S. & GLATZMAIER, G. A. 2010 Dynamo models for planets other than Earth. *Space Sci. Rev.* **152**, 617–649.
- STEENBECK, M. & KRAUSE, F. 1966 The generation of stellar and planetary magnetic fields by turbulent dynamo action. *Z. Naturforsch.* **21a**, 1285–1296.
- STEENBECK, M., KRAUSE, F. & RÄDLER, K.-H. 1966 A calculation of the mean electromotive force in an electrically conducting fluid in turbulent motion, under the influence of coriolis forces. *Z. Naturforsch.* **21a**, 369–376.
- STELLMACH, S. & HANSEN, U. 2004 Cartesian convection driven dynamos at low Ekman number. *Phys. Rev. E* **70** (056312).
- STELLMACH, S., LISCHPER, M., JULIEN, K., VASIL, G., CHENG, J. S., RIBEIRO, A., KING, E. M. & AURNOU, J. M. 2014 Approaching the asymptotic regime of rapidly rotating convection: boundary layers versus interior dynamics. *Phys. Rev. Lett.* **113** (254501).
- VASIL, G. M., LECOANET, D., BROWN, B. P., WOOD, T. S. & ZWEIBEL, E. G. 2013 Energy conservation and gravity waves in sound-proof treatments of stellar interiors. II. Lagrangian constrained analysis. *Astrophys. J* **773**, 169.
- WELANDER, P. 1959 An advective model for the ocean thermocline. *Tellus* **11**, 309–318.